Letter

Out-of-equilibrium Majorana zero modes in interacting Kitaev chains

Bradraj Pandey, Narayan Mohanta, and Elbio Dagotto
Department of Physics and Astronomy, University of Tennessee, Knoxville, Tennessee 37996, USA
and Materials Science and Technology Division, Oak Ridge National Laboratory, Oak Ridge, Tennessee 37831, USA

(Received 7 September 2022; revised 7 December 2022; accepted 7 February 2023; published 15 February 2023)

We employ a time-dependent real-space local density-of-states method to study the movement and fusion of Majorana zero modes in the one-dimensional interacting Kitaev model, based on the time evolution of many-body states. We analyze the dynamics and both fusion channels of Majoranas using time-dependent potentials, either creating walls or wells. For fast moving Majoranas, we unveil nonequilibrium signatures of the "strong-zero-mode" operator (quasiparity degeneracy in the full spectrum) and its breakdown in the presence of repulsive Coulomb interactions. Focusing on forming a full electron after fusion, we also discuss the upper and lower limits on the Majorana speed needed to reduce nonadiabatic effects and to avoid poisoning due to decoherence.

DOI: 10.1103/PhysRevB.107.L060304

Introduction. Majorana zero modes (MZMs) generate considerable interest because of potential applications in quantum information and computation [1–3]. MZMs obey non-Abelian exchange statistics. Because they are topologically protected from local perturbations and disorder, they are of value as possible qubits [4–6]. Signatures of MZMs are expected to develop in tunneling conductance experiments as zero-bias peaks [7–9]. The simplest setup to realize Majoranas are quantum wires, where MZMs develop at the two edges [1,10]. For ferromagnetic atomic chains with strong spin-orbit coupling placed over a superconductor, MZMs were indeed reported at the edges in spatially and spectrally resolved scanning tunneling experiments [11,12]. In nanowires, most theoretical work neglects repulsion among particles. However, Coulomb repulsion plays an important role in one-dimensional (1D) MZMs because it suppresses the pairing-induced bulk gap and can destroy topological protection [13,14].

The movement of Majoranas and detection of fusion channels are important for quantum-information processing [10,15]. MZMs behave as Ising non-Abelian anyons [4,16] and obey the fusion rule [15], $\gamma \times \gamma = I + \psi$, meaning two MZMs can fuse into the vacuum I or into an electron ψ. The fusion process requires a slow adiabatic movement of Majoranas, achieved by applying properly adjusted time-dependent local gates to the topological superconducting wire [10]. The rapid progress in quantum wires with tunable local gates [10,15,17] provides a promising platform for the creation, movement, and fusion of Majoranas [18].

Motivated by experimental progress in nanowires [19], here we employ a computationally intensive time-dependent real-space local density-of-states LDOS(ω, j, t) method to observe the movement and fusion of Majoranas in the interacting Kitaev model. The uniqueness of our effort is that we can study Majorana movement at *any* speed by properly choosing the time dependence of gate voltages, namely we can access the nonequilibrium situation away from adiabaticity, difficult to reach by theoretical tools. The LDOS(ω, j, t) of moving Majoranas and fusion outcome can be measured in tunneling spectroscopy experiments based on gate-controlled nanowire devices [19,20]. Compared to previous studies based on single-particle states, here we use the exact-diagonalization method for the time evolution of the many-body states of *interacting* electrons in a 1D Kitaev model up to 16 sites. We address the out-of-equilibrium properties and fusion rules of MZMs via the sequential application of time-dependent chemical potential gates. For fast moving noninteracting MZMs, using the time-dependent LDOS, we find the signature of a "strong-zero-mode" operator in LDOS(ω, j, t) [21,22]. Remarkably, we found the total spectral weight at $\omega = 0$ remains conserved (almost identical to the case of slow moving Majoranas). However, with interaction V, depending on its strength and switching time τ, we find a loss in spectral weight at $\omega = 0$ and a breakdown of the strong-zero-mode properties. Furthermore, we provide the timescale to observe the fusion rules of interacting Majoranas. Although it is widely expected that for the "adiabatic" movement of MZMs their fusion will lead to the formation of a fermion or vacuum states, only by the use of calculations as presented here, that allow for *any* speed for the MZMs, can we establish how "slow" the movement must truly be in practice.

Model and method. We consider the time-dependent interacting 1D Kitaev model for spinless fermions with open boundary conditions to anchor MZMs,

$$H(t) = -t_h \sum_{i=1}^{N-1} (c_i^\dagger c_{i+1} + \text{H.c.}) + V \sum_{i=1}^{N-1} (n_i n_{i+1}) + \Delta \sum_{i=1}^{N-1} (c_i c_{i+1} + \text{H.c.}) + \sum_{i}^{N} \mu_i(t) n_i, \quad (1)$$

where $n_i = c_i^\dagger c_i$ and $c_i^\dagger$ (c_i) is the fermionic creation (annihilation) operator, t_h is the hopping amplitude, and Δ is

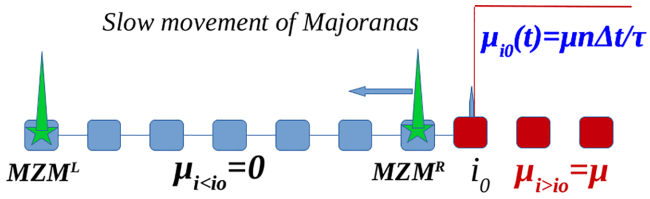

FIG. 1. Schematic representation of the transfer of the right edge MZM^R to site $i_0 - 1$ in a 1D Kitaev chain. The on-site chemical potential at any site can be tuned using time-dependent local gates with quench rate $1/\tau$. Large (small) τ corresponds to the slow (fast) motion of MZM^R. Blue squares denote the topological region (with $\mu_{i<i_0} = 0$) while red squares denotes the nontopological region (with $\mu_{i>i_0} = \mu$) for this wall case. For the well, the red region has a negative μ.

the p-wave pairing strength. The time-dependent Hamiltonian $H(t)$ [Eq. (1)] commutes with the parity operator $P = e^{i\pi \sum_j n_j}$ [23,24]. The time dependence is incorporated in the chemical potential $\mu_i(t)$ as

$$\mu_i(t) = 0 \ (i < i_0), \quad \mu_i(t) = \mu \ (i > i_0),$$
$$\mu_i(t) = \mu \frac{n\Delta t}{\tau} \ (i = i_0), \tag{2}$$

where $1/\tau$ is the quenched rate, $\Delta t = 0.001$ is the small time step we used, and n is the integer number of those steps, such that the on-site chemical potential $\mu_i(t)$ at $i = i_0$ increases approximately linearly from 0 to μ in a time τ (defined as the switching time of the local gate at site $i = i_0$). The sequential application of on-site gates $\mu_i(t)$ on the right half of the 1D chain creates a moving wall for $\mu > 0$ (or moving well for $\mu < 0$), separating topological from nontopological regions at site $i = i_0$. Equating our number of sites with the number of gates in a coarse-grained approach, this process leads to the movement of the right edge Majorana zero mode (MZM^R) from the edge $i = N$ to site $i_0 - 1$ in a finite time $t = N_R\tau$, with N_R the number of sites where the chemical potential reaches its maximum value (here being $|\mu| = 12$) at time t (Fig. 1).

To calculate the time-dependent local density of states (at zero temperature), we first time evolve the ground-state wave function $|\psi(0)\rangle$ up to time $t = N_R\tau$, using the time-dependent Hamiltonian $H(t)$ as $|\Psi(t)\rangle = \mathcal{T} \exp(-i \int_0^t H(s)ds)|\psi(0)\rangle$, where $\mathcal{T}$ is the time ordering operator [25]. Then, we calculate the double-time Green's function $G(t, t')$ [26], using the time-independent Hamiltonian $H_f = H(t = t_f)$ at time $t_f = N_R\tau$:

$$G_j^{\rm elec}(t, t') = \langle \Psi(t)|c_j^\dagger e^{iH_f t'} c_j e^{-iH_f t'}|\Psi(t)\rangle. \tag{3}$$

The time-dependent $\mathrm{LDOS}_{\rm elec}(\omega, j, t)$ for electrons is a Fourier transform with respect to t' of the local Green's function at site j,

$$\mathrm{LDOS}_{\rm elec}(\omega, j, t) = \frac{1}{\pi}\mathrm{Im} \int_0^T dt' e^{i(\omega+i\eta)t'} iG_j^{\rm elec}(t, t'), \tag{4}$$

where we use $T = 70$ for the integration, and broadening $\eta = 0.1$. Similarly we obtained the $\mathrm{LDOS}_{\rm hole}(\omega, j, t)$ for holes, using the Fourier transform of the Green's function $G_j^{\rm hole}(t, t') = \langle \Psi(t)|c_j(t')c_j^\dagger|\Psi(t)\rangle$. The total local density of states at site j is thus $\mathrm{LDOS}(\omega, j, t) = \mathrm{LDOS}_{\rm hole}(\omega, j, t) + \mathrm{LDOS}_{\rm elec}(\omega, j, t)$.

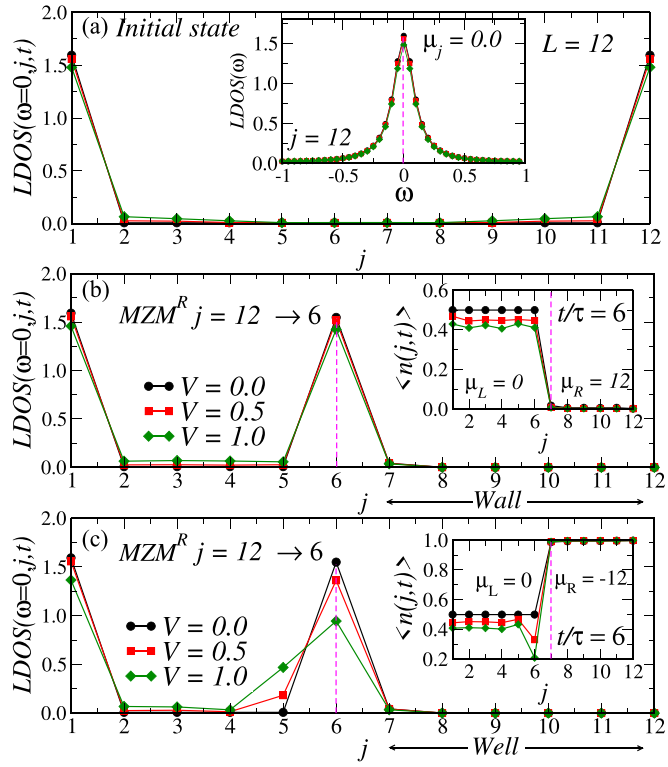

FIG. 2. Slow movement of Majoranas. (a) Local density of states $\mathrm{LDOS}(j, \omega, t)$ vs site j, at time $t = 0$ and for $\omega = 0$. The sharp peaks at sites $j = 1$ and $j = 12$ in $\mathrm{LDOS}(j, \omega = 0, t)$ represent Majorana edge modes for different values of V and $\mu_j = 0$ (for $1 < j < 12$). Inset: $\mathrm{LDOS}(\omega)$ vs ω at site $j = 12$ using broadening $\eta = 0.1$. Site-dependent $\mathrm{LDOS}(j, \omega, t)$ at $\omega = 0$ and time $t/\tau = 6$ for $V = 0$, 0.5, and 1.0 with $\tau = 36$, 60, and 72, respectively, for (b) positive μ (wall). The inset shows the site-dependent density $\langle n(j, t)\rangle$ at $t/\tau = 6$ for $\mu_R = 12$. (c) Negative μ (well). The inset shows the site-dependent density $\langle n(j, t)\rangle$ at time $t/\tau = 6$ for $\mu_R = -12$. $L = 12$ sites and $t_h = \Delta = 1.0$ were used.

Slow movement of Majoranas. For fusion or braiding of MZMs, it is required to transfer the Majoranas slowly, close to the adiabatic limit [27,28]. Figure 2(a) shows the real-space local density of states $\mathrm{LDOS}(\omega = 0, j, t = 0)$ vs site j, with $\mu_i = 0$ (for all sites), and at $t_h = \Delta = 1$. For small or zero V, these peaks are sharply localized at the end sites ($i = 1$ and 12), whereas for robust V the $\omega = 0$ peaks are slightly delocalized over a few sites. In the inset, we show $\mathrm{LDOS}(\omega)$ at time $t = 0$ at the end site $j = 12$ and several V's. We find a sharp peak at $\omega = 0$, signaling a MZM mode at the end site. Integrating in ω the $\mathrm{LDOS}(\omega, j = 12)$ at $V = 0.0$ gives a spectral weight of 0.48, close to the analytically expected value of 0.5 [29].

Next, with the sequential application of the time-dependent chemical potential $\mu_j(t)$, the right edge MZM^R (at site $j = 12$) is moved to the middle site ($j = 6$) in a time $t = N_R\tau$ (i.e., $t/\tau = N_R = 6$ because we travel six sites). We study cases $\tau = 36$, 60, and 72, for interaction strengths $V = 0.0$, 0.5, and 1.0, respectively. In this case, $|\psi(t)\rangle$ remains close to the degenerate ground-state space [larger values of V require

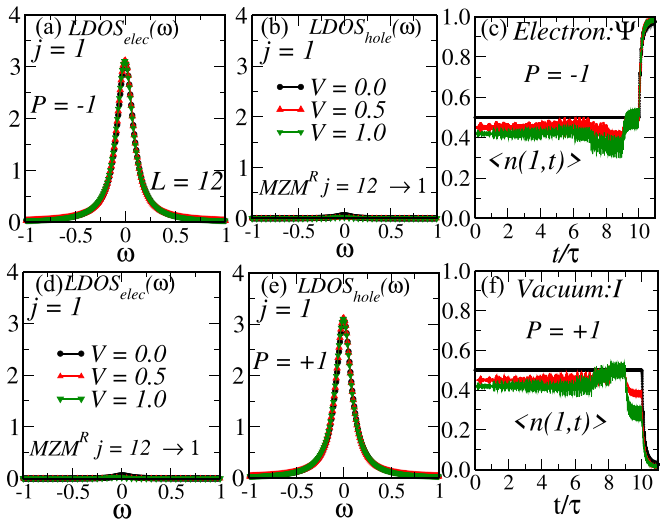

FIG. 3. Slow Majorana fusion using $\mu(t) > 0$ (wall), $\Delta = 1$, at $V = 0.0$, 0.5, and 1.0, with $\tau = 36$, 60, and 72, respectively. The upper panels show Majorana fusion for the initial state with parity $P = -1$. (a) Electron $\mathrm{LDOS}_{\mathrm{elec}}(\omega)$ after moving a MZM from $j = 12$ to $j = 1$. (b) Hole $\mathrm{LDOS}_{\mathrm{hole}}(\omega)$ at $t/\tau = 11$ and site $j = 1$. (c) Charge density $\langle n(j = 1, t)\rangle$ vs time t, varying V. The lower panels show Majorana fusion for the initial state with parity $P = +1$. (d) Electron $\mathrm{LDOS}_{\mathrm{elec}}(\omega)$ at $t/\tau = 11$ and site $j = 1$. (e) Hole $\mathrm{LDOS}_{\mathrm{hole}}(\omega)$ after moving a MZM from $j = 12$ to $j = 1$. (f) Charge density $\langle n(j = 1, t)\rangle$ vs time t.

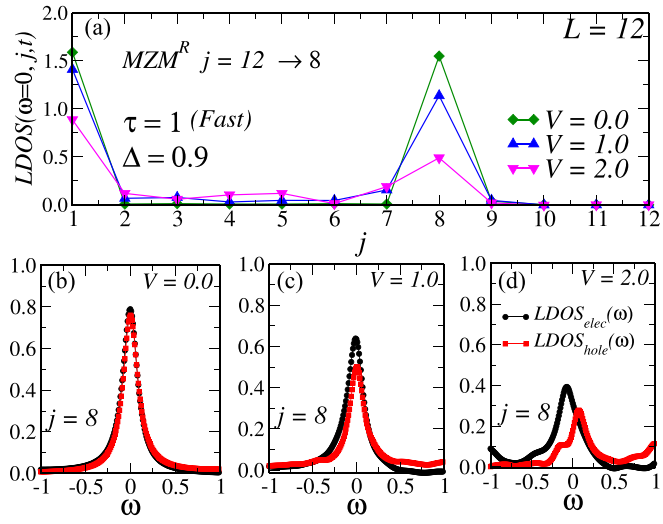

FIG. 4. Fast movement of Majoranas using a small quench rate $\tau = 1$, $\mu(t) > 0$ (wall), and for the initial state with parity $P = -1$. (a) Site-dependent $\mathrm{LDOS}(j, \omega, t)$ at $\omega = 0$, for $V = 0.0$, 1.0, and 2.0, after moving the right MZM from site 12 to 8. Electron $\mathrm{LDOS}_{\mathrm{elec}}(\omega)$ and hole $\mathrm{LDOS}_{\mathrm{elec}}(\omega)$ at site $j = 8$, for (b) $V = 0.0$, (c) $V = 1.0$, and (d) $V = 2.0$.

a slower rate of increase in the on-site $\mu_{i_0}(t)$]. As shown in Fig. 2(b), for $\mu = 12$ (i.e., when creating a potential wall), the $\mathrm{LDOS}(\omega = 0, j, t)$ has peaks at sites $j = 1$ and $j = 6$ at time $t/\tau = 6$, indicating that a slow transfer of MZM^R from $j = 12$ to $j = 6$ occurred. The average density $\langle n(j, t)\rangle$ is close to zero for $j \geqslant 7$, while it is close to 0.5 for $j \leqslant 6$ [inset of Fig. 2(b)]. Interestingly, at $\mu_R = -12$ (when creating a potential well), the effect of interaction increases. In the nontopological region ($j \geqslant 7$), each site is occupied by one fermion, whereas in the topological region ($j \leqslant 6$) the mean occupancy is close to 0.5. With nonzero V, to minimize the Coulomb interaction between fermions at the topological to nontopological boundary, the fermions near the boundary become inhomogeneously distributed [Fig. 2(c) inset]. This delocalizes MZM^R over more sites as V increases [Fig. 2(c)].

Slow fusion of Majoranas. For the fusion of Majoranas, we move the right edge MZM^R slowly all the way to the left end (site $j = 1$) using sequential operations of $\mu(t)$ in a time interval $t = 11\tau$ (see the caption of Fig. 3). At $t = 0$, for $V = 0$, $t_h = \Delta = 1$, with $\mu_i = 0$ (for all sites), the system has degenerate many-body ground states ($|\psi_1\rangle$ and $|\psi_2\rangle$). These degenerate ground states have a different fermionic parity $P = \pm 1$. At $t = 0$, we start the time evolution with those initial states $|\psi_s\rangle$ ($s = 1$ or 2) up to $t/\tau = 11$, to confirm both fusion channels (electron : Ψ and vacuum : I). For a positive chemical potential, $\mu(t) > 0$ (wall) and the initial states $|\psi_s\rangle$ with parity $P = -1$, the electron $\mathrm{LDOS}_{\mathrm{elec}}(\omega)$ at $j = 1$ shows a sharp peak close to $\omega = 0$, for $V = 0$, 0.5, and 1 [Fig. 3(a)]. Meanwhile, the hole $\mathrm{LDOS}_{\mathrm{hole}}(\omega)$ at $j = 1$, displays no peak [Fig. 3(b)]. The time-dependent density $\langle n(j = 1, t)\rangle$ at site $j = 1$ takes a value of 1 at $t/\tau = 11$, giving a clear indication of the formation of a single electron (spinless) at site $j = 1$ after Majorana fusion [Fig. 3(c)]. On the other hand, for the initial state $|\psi_s\rangle$ with parity $P = +1$, the hole $\mathrm{LDOS}_{\mathrm{hole}}(\omega)$ displays a sharp peak close to $\omega = 0$, for $V = 0$, 0.5, and 1 [Fig. 3(e)]. The electron $\mathrm{LDOS}_{\mathrm{elec}}(\omega)$ has no peak at $t/\tau = 11$ [see Fig. 3(d)]. The density $\langle n(j = 1, t)\rangle$ at $j = 1$ approaches zero [Fig. 3(f)], confirming a vacuum state at $t/\tau = 11$. Because the MZM spreads over more than one site as V grows, density fluctuations occur at site $j = 1$ as compared to $V = 0$ [Figs. 3(c) and 3(f)] (for the slow fusion of Majoranas, in the presence of a time-dependent potential well, see the Supplemental Material [30]).

Fast movement of Majoranas. Changing $\mu(t)$ employing a faster rate (smaller τ) leads to a fast movement of MZMs^R generating nonadiabatic effects [31,32]. The faster change in $\mu(t)$ results in a finite overlap of the time-evolving wave function $|\psi(t)\rangle$ with excited states of the instantaneous Hamiltonian $H(t)$. Starting the time evolution with initial states $|\psi_s\rangle$, with parity $P = -1$ for $\mu(t) > 0$ (wall) and using all eigenvectors $\{|n\rangle\}$ of the instantaneous Hamiltonian $H(t)$, the electron LDOS at finite time $t = N_R\tau$ can be written as

$$\mathrm{LDOS}_{\mathrm{elec}}(\omega, t) = \frac{-1}{\pi}\mathrm{Im}\left(\sum_{m,n}\frac{\langle\Psi(t)|c_j^+|n\rangle\langle n|c_j|m\rangle\langle m|\Psi(t)\rangle}{e_n - e_m + \omega + i\eta}\right), \quad (5)$$

where $\eta = 0.1$, and the rest of the notation is standard (as a reference for $L = 12$ the number of states is 4096).

Figure 4(a) shows $\mathrm{LDOS}(\omega, j, t)$ after moving the MZM from $j = 12$ to $j = 8$ for different values of Coulomb interaction V and with a fast quench rate $\tau = 1$. For $V = 0$, and for this faster change in $\mu(t)$ the peak values of $\mathrm{LDOS}(\omega, j, t)$ almost remain the same as compared to slower changes in $\mu(t)$ [Fig. 2(b)]. On the other hand, for the same faster moving MZMs but for a finite repulsion V, there is a significant

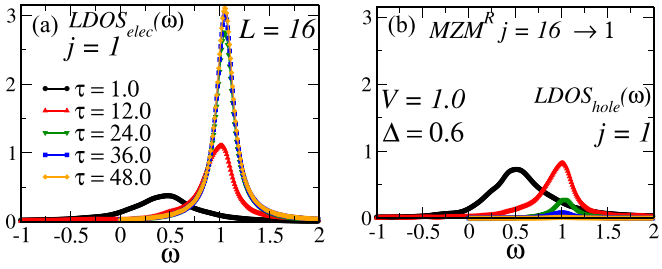

FIG. 5. Fast Majorana fusion using $\mu(t) < 0$ (well) at various τ's, for the initial state with $P = +1$. The right MZM is moved from site $j = 16$ to 1. (a) $\mathrm{LDOS}_{\mathrm{elec}}(\omega)$ at site $j = 1$ and (b) $\mathrm{LDOS}_{\mathrm{hole}}(\omega)$ at $j = 1$, for $V = 1$, $\Delta = 0.6$, and $L = 16$.

reduction in the peaks' magnitude of $\mathrm{LDOS}(\omega, j, t)$ (at sites $j = 1$ and $j = 8$) with increasing V. For larger values of V, the site-dependent $\mathrm{LDOS}(\omega, j, t)$ indicate a finite overlap between the left and right MZMs [Fig. 4(a)]. Figures 4(b)–4(d) contain the electron $\mathrm{LDOS}_{\mathrm{elec}}(\omega)$ and hole $\mathrm{LDOS}_{\mathrm{hole}}(\omega)$ vs ω at site $j = 8$, for different values of the Coulomb interaction V at time $t/\tau = 4$. Using full diagonalization of $H(t)$, we find for $V = 0$ and $\Delta = 0.9$ [33] that all many-body eigenstates of $H(t)$ come in pairs with opposite parity $P = \pm 1$ and the states of each pair are almost degenerate (the parity degeneracy of all many-body states is compatible with a strong-zero-mode operator [21,22]). The equal peak heights of $\mathrm{LDOS}_{\mathrm{elec}}(\omega, t)$ and $\mathrm{LDOS}_{\mathrm{hole}}(\omega, t)$ at $\omega = 0$ in Fig. 4(b) (with spectral weight 0.5) can be associated with the presence of such a strong-zero-mode operator when in nonequilibrium. The spectral weight is dominated by only a few higher-energy degenerate-pair states, all with a comparable weight, contributing to $\omega = e_n - e_m = 0$ (with $|m - n| = 1$) in the $\mathrm{LDOS}_{\mathrm{elec}}(\omega, t)$ [Eq. (6)] and $\mathrm{LDOS}_{\mathrm{hole}}(\omega, t)$.

This strong-zero-mode operator is immune to decoherence [34], potentially leading to topological qubits with infinite coherence time [35]. This occurs because they are topologically protected due to global parity conservation and quasidegenerate paired states in the full spectrum (involving opposite fermion parity) [21,36]. This protection survives as long as the left and right MZMs do not overlap with each other. However, increasing V, the peaks of $\mathrm{LDOS}_{\mathrm{elec}}(\omega, t)$ and $\mathrm{LDOS}_{\mathrm{hole}}(\omega, t)$ start splitting and the peak values are no longer equal in magnitude [Figs. 4(c) and 4(d)]. Furthermore, at large V the electron and hole parts of LDOS show peaks away from zero and these peaks are largely split. The split in the $\mathrm{LDOS}_{\mathrm{elec}}(\omega, t)$ and $\mathrm{LDOS}_{\mathrm{hole}}(\omega, t)$ peaks is due to the breakdown of degeneracy of higher excited paired states increasing V.

Fast fusion of Majoranas. In real Majorana nanowire setups, it is necessary to move the Majoranas with sufficient speed to be faster than the quasiparticle "poisoning" time [15,37–39]. Here, we present the minimum required switching time of local gates for fast moving MZM^R, so that we obtain a full electron after the fusion of left and right MZMs. To fuse Majoranas, starting with the initial state having parity $P = +1$, we moved at various speeds the right MZM^R all the way to the left end (site $j = 1$).

In Figs. 5(a) and 5(b), we show the fusion of Majoranas using a potential well [$\mu(t) < 0$] with $\Delta = 0.6$, $V = 1$, and for the system length $L = 16$. For these parameters, we believe our system is closer to realistic setups [40] for experiments [11,12]. However, for a negative chemical potential, after the formation of an electron at site $j = 1$, the repulsive nearest-neighbor V leads to the split in the ground-state energy (approximately of order V [30]), causing an energy shift in the peak values of $\mathrm{LDOS}_{\mathrm{elec}}(\omega)$ and $\mathrm{LDOS}_{\mathrm{hole}}(\omega)$ increasing τ. Also, increasing τ (slower motion of MZM^R), the peak at $\omega = V$ for $\mathrm{LDOS}_{\mathrm{elec}}(\omega)$ starts increasing, while the $\mathrm{LDOS}_{\mathrm{hole}}(\omega)$ peak value at $\omega = V$ decreases. At $\tau = 48$, we obtain a sharp electron peak close to $\omega = 1.0$, whereas the $\mathrm{LDOS}_{\mathrm{hole}}(\omega)$ peak vanishes to zero as τ grows [Figs. 5(a) and 5(b)]. Specifically, this shows the formation of a full electron at $\tau = 48$ for $\Delta = 0.6$, $V = 1$, and $L = 16$.

In terms of SI units, the switching time per gate for $V = 1$ corresponds to $\tau\hbar/\Delta \sim 0.17$–$5.2$ ns (using $\tau = 48$, and $\Delta = 180$ μeV or $\Delta = 6$ μeV as in previous literature [18,37]). Independently, the quasiparticle "poisoning" time in nanowire systems has been estimated in a broad range 10 ns to 10 ms [37,38]. Because in the worse case of 5.2 ns, eight gates require a total time 41.6 ns to move adiabatically the Majorana, and since this number is close to the poisoning time, we conclude that there should be a time range where moving Majoranas in chains can occur adiabatically before poisoning occurs for $V = 1$. As V increases, the situation deteriorates because we must use larger τ to form a full electron after fusion (see Supplemental Material for larger V [30]).

Conclusions. We performed real-time dynamics and fusion of Majoranas in the interacting 1D Kitaev model using a sequential application of time-dependent chemical potentials (gates). We show that the movement and fusion outcomes can be monitored using the time-dependent local density of states, and should be observed in tunneling spectroscopy experiments [19]. We find that for noninteracting and fast moving Majoranas, the near degeneracy of MZMs exists even in many higher-energy states and MZMs remain topologically protected. However, for the interacting case, with increasing V we find a decrease in spectral weight at $\omega = 0$ in the time-dependent local density of states. Furthermore, we estimate the minimum required switching time of local gates to form a full electron after the fusion. Due to advancements in fabricating Majorana nanowires [19,41] with long quasiparticle poisoning times [37,38], and considering our estimations for the times needed for adiabatic movement, we believe proper Majorana movement could be realized in realistic gate-controlled nanowire devices [19,20,42].

Note added. Recently, we became aware of an experimental realization of the two-site Kitaev chain employing two quantum dots coupled through a short superconducting semiconducting hybrid (InSb nanowires) [43]. In this experiment, the authors were able to tune the hopping (t_h) and pairing term Δ close to $t_h = \Delta$. Interestingly, using tunneling spectroscopy measurements they showed the signature of two localized Majorana modes on each quantum dot close to $t_h = \Delta$. This experimental realization of a minimal Kitaev chain opens the possibility of an experimental confirmation of our predictions about Majorana fusion (at $t_h \sim \Delta$) using arrays of quantum dots.

Acknowledgment. B.P., N.M., and E.D. were supported by the U.S. Department of Energy (DOE), Office of Science, Basic Energy Sciences (BES), Materials Sciences and Engineering Division.

[1] A. Y. Kitaev, Phys. Usp. **44**, 131 (2001).
[2] M. H. Freedman, A. Kitaev, M. J. Larsen, and Z. Wang, Bull. Am. Math. Soc. **40**, 31 (2003).
[3] P. Bonderson, M. Freedman, and C. Nayak, Phys. Rev. Lett. **101**, 010501 (2008).
[4] C. Nayak, S. H. Simon, A. Stem, M. Freedman, and S. Das Sarma, Rev. Mod. Phys. **80**, 1083 (2008).
[5] N. Mohanta, S. Okamoto, and E. Dagotto, Commun. Phys. **4**, 163 (2021).
[6] S. D. Sarma, M. Freedman, and C. Nayak, npj Quantum Inf. **1**, 15001 (2015).
[7] C. J. Bolech and E. Demler, Phys. Rev. Lett. **98**, 237002 (2007).
[8] M. T. Deng, S. Vaitiekėnas, E. B. Hansen, J. Danon, M. Leijnse, K. Flensberg, J. Nygård, P. Krogstrup, and C. M. Marcus, Science **354**, 1557 (2016).
[9] D. Wang, L. Kong, P. Fan, H. Chen, S. Zhu, W. Liu, Lu Cao, Y. Sun, S. Du, J. Schneeloch, R. Zhong, G. Gu, L. Fu, H. Ding, and H.-J. Gao, Science **362**, 333 (2018).
[10] J. Alicea, Y. Oreg, G. Refael, F. von Oppen, and M. P. A. Fisher, Nat. Phys. **7**, 412 (2011).
[11] S. Nadj-Perge, I. K. Drozdov, J. Li, H. Chen, S. Jeon, J. Seo, A. H. MacDonald, B. A. Bernevig, and A. Yazdani, Science **346**, 602 (2014).
[12] B. E. Feldman, M. T. Randeria, J. Li, S. Jeon, Y. Xie, Z. Wang, I. K. Drozdov, B. A. Bernevig, and A. Yazdani, Nat. Phys. **13**, 286 (2017).
[13] S. Gangadharaiah, B. Braunecker, P. Simon, and D. Loss, Phys. Rev. Lett. **107**, 036801 (2011).
[14] R. Thomale, S. Rachel, and P. Schmitteckert, Phys. Rev. B **88**, 161103(R) (2013).
[15] D. Aasen, M. Hell, R. V. Mishmash, A. Higginbotham, J. Danon, M. Leijnse, T. S. Jespersen, J. A. Folk, C. M. Marcus, K. Flensberg, and J. Alicea, Phys. Rev. X **6**, 031016 (2016).
[16] E. Grosfeld and K. Schoutens, Phys. Rev. Lett. **103**, 076803 (2009).
[17] M. C. Dartiailh, W. Mayer, J. Yuan, K. S. Wickramasinghe, A. Matos-Abiague, I. Žuticć, and J. Shabani, Phys. Rev. Lett. **126**, 036802 (2021).
[18] T. Zhou, M. C. Dartiailh, K. Sardashti, J. E. Han, A. Matos-Abiague, J. Shabani and I. Žutić, Nat. Commun. **13**, 1738 (2022).
[19] H. Zhang, D. E. Liu, M. Wimmer, and L. P. Kouwenhoven, Nat. Commun. **10**, 5128 (2019).
[20] D. I. Pikulin, B. van Heck, T. Karzig, E. A. Martinez, B. Nijholt, T. Laeven, G. W. Winkler, J. D. Watson, S. Heedt, M. Temurhan, V. Svidenko, R. M. Lutchyn, M. Thomas, G. de Lange, L. Casparis, and C. Nayak, arXiv:2103.12217.
[21] G. Kells, Phys. Rev. B **92**, 081401(R) (2015).
[22] P. Fendley, J. Phys. A: Math. Theor. **49**, 30LT01 (2016).
[23] J.-J. Miao, H.-K. Jin, F.-C. Zhang, and Y. Zhou, Sci. Rep. **8**, 488 (2018).
[24] A. M. Turner, F. Pollmann, and E. Berg, Phys. Rev. B **83**, 075102 (2011).
[25] G. Kells, D. Sen, J. K. Slingerland, and S. Vishveshwara, Phys. Rev. B **89**, 235130 (2014).
[26] D. M. Kennes, C. Klöckner, and V. Meden, Phys. Rev. Lett. **113**, 116401 (2014).
[27] T. Karzig, A. Rahmani, F. von Oppen, and G. Refael, Phys. Rev. B **91**, 201404(R) (2015).
[28] L. Coopmans, D. Luo, G. Kells, B. K. Clark, and J. Carrasquilla, PRX Quantum **2**, 020332 (2021).
[29] The value 0.48 instead of 0.5 of spectral weight might arise from an integration error due to finite ω steps and the broadening η used.
[30] See Supplemental Material at http://link.aps.org/supplemental/10.1103/PhysRevB.107.L060304 for the analytical calculations.
[31] M. S. Scheurer and A. Shnirman, Phys. Rev. B **88**, 064515 (2013).
[32] A. Conlon, D. Pellegrino, J. K. Slingerland, S. Dooley, and G. Kells, Phys. Rev. B **100**, 134307 (2019).
[33] For $t_h = \Delta = 1$, the system has many states with the same energy above the gap and we are not able to calculate the parity of these high-energy states. However, the electron and hole components of LDOS(ω, j, t) remain the same for fast moving Majoranas.
[34] G. Goldstein and C. Chamon, Phys. Rev. B **86**, 115122 (2012).
[35] N. Laflorencie, G. Lemarié, and N. Macé, Phys. Rev. Res. **4**, L032016 (2022).
[36] A. R. Akhmerov, Phys. Rev. B **82**, 020509(R) (2010).
[37] A. P. Higginbotham, S. M. Albrecht, G. Kirsanskas, W. Chang, F. Kuemmeth, P. Krogstrup, T. S. Jespersen, J. Nygard, K. Flensberg, and C. M. Marcus, Nat. Phys. **11**, 1017 (2015).
[38] D. Rainis and D. Loss, Phys. Rev. B **85**, 174533 (2012).
[39] G. Goldstein and C. Chamon, Phys. Rev. B **84**, 205109 (2011).
[40] J. Herbrych, M. Środa, G. Alvarez, M. Mierzejewski, and E. Dagotto, Nat. Commun. **12**, 2955 (2021).
[41] P. Krogstrup, N. L. B. Ziino, W. Chang, S. M. Albrecht, M. H. Madsen, E. Johnson, J. Nygård, C. M. Marcus, and T. S. Jespersen, Nat. Mater. **14**, 400 (2015).
[42] Using the time-dependent local density-of-states method, we plan to work out of equilibrium, addressing fusion and strong zero modes, in the interacting Kitaev model also in the presence of *quenched disorder*. See, for example, H. Pan and S. Das Sarma, Phys. Rev. B **103**, 195158 (2021); the computational techniques used in our effort are capable of addressing such a challenging combination of Majoranas, time dependence, and disorder.
[43] T. Dvir, G. Wang, N. van Loo, C.-X. Liu, G. P. Mazur, A. Bordin, S. L. D. ten Haaf, J.-Y. Wang, D. van Driel, F. Zatelli, X. Li, F. K. Malinowski, S. Gazibegovic, G. Badawy, E. P. A. M. Bakkers, M. Wimmer, and L. P. Kouwenhoven, arXiv:2206.08045.